metals

MDPI

Article

Research Progress of Corrosion Induced by Second-Phase Particles in Microalloyed High-Strength Rebars—Review

Shiwang Li [1,2], Changrong Li [1,2,*], Zeyun Zeng [1,2], Changling Zhuang [1,2], Sheng Huang [1,2] and Jingtian You [1,2]

[1] College of Materials and Metallurgy, Guizhou University, Guiyang 550025, China; li1255182645@163.com (S.L.); zzy19950406@163.com (Z.Z.); clzhuang@gzu.edu.cn (C.Z.); hs19967691957@163.com (S.H.); youjt7@163.com (J.Y.)

[2] Guizhou Key Laboratory of Metallurgical Engineering and Process Energy Conservation, Guiyang 550025, China

* Correspondence: crli@gzu.edu.cn

Abstract: The research progress surrounding second-phase particle-induced corrosion has been expounded through extensive work, including local corrosion (pitting corrosion, crevice corrosion, stress corrosion) of Al_2O_3, (RE)-AlO_3, CaS, MnS, NbC, and other particles in microalloyed high-strength rebars. By summarizing the local corrosion mechanism of these particle-induced rebars, this review further explores the fact that these particles play an inducing role in the local corrosion of microalloyed high-strength rebars, which has guiding significance for research on the induced corrosion of microalloyed high-strength rebars.

Keywords: Al_2O_3 inclusion; carbonitride; sulfide inclusion; local corrosion

check for updates

Citation: Li, S.; Li, C.; Zeng, Z.; Zhuang, C.; Huang, S.; You, J. Research Progress of Corrosion Induced by Second-Phase Particles in Microalloyed High-Strength Rebars—Review. *Metals* **2022**, *12*, 925. https://doi.org/10.3390/met12060925

Academic Editor: Frank Czerwinski

Received: 11 March 2022
Accepted: 4 May 2022
Published: 27 May 2022

Publisher's Note: MDPI stays neutral with regard to jurisdictional claims in published maps and institutional affiliations.

Copyright: © 2022 by the authors. Licensee MDPI, Basel, Switzerland. This article is an open access article distributed under the terms and conditions of the Creative Commons Attribution (CC BY) license (https://creativecommons.org/licenses/by/4.0/).

1. Introduction

Reinforced concrete structures are widely used in civil engineering. Due to the damage to material properties, improper use methods and conditions, and the failure of material structure caused by the use conditions, steel corrosion has become a common phenomenon in reinforced concrete structures [1]. This reduces the usability and durability of reinforced concrete structures in civil engineering, resulting in structural failure and even collapse accidents. Additionally, the corrosion failure of steel structures also indirectly causes huge economic losses [2]. According to incomplete data statistics, the economic losses caused by steel structure corrosion each year account for 2–4% of the total national economic value, which is equivalent to the annual Gross Domestic Product (GDP) of the UK. Rebars corrosion has become a serious worldwide problem [3].

In recent years, efforts have been carried out both at home and abroad to improve the corrosion resistance of steel bars. At the same time, the monitoring corrosion rate model has also been used to preform extensive theoretical exploration and experimental research, and to develop empirical models, reaction control models, and electrochemical models. Electrochemical models are often used to establish corrosion rate models and predict the durability of reinforced concrete structures, and linear polarization and polarization resistance are commonly used in electrochemical models. Li et al. [4] found that the corrosion rates of high-strength, low-alloy steel were significantly accelerated in the case of hydrogen charging through the polarization curve study. Wang et al. [5] found that the increase in HCO_3^-/CO_3^{2-} concentration accelerated the dissolution process of the passive film and caused steel corrosion by using polarization curves and electrochemical impedance spectroscopy.

The main environmental factor causing rebar corrosion is salt damage, and salt-intensive environments are mainly marine, coastal, and seawater environments. The salt in seawater is mainly chloride salt. In the marine environment, chloride ions easily penetrate and diffuse from concrete to the surface of rebars, which causes local corrosion of rebars.

Some studies have shown that local corrosion is the main reason for the degradation of concrete reinforcement structures in the marine environment [6,7]. Local corrosion mainly includes pitting corrosion, crevice corrosion, stress corrosion, and grain boundary corrosion. Pitting corrosion is the most common corrosion form of low-carbon steel and microalloys, which is the main corrosion source for local corrosion of rebars. Pitting corrosion usually occurs in the surface chemical or physical uneven positions of inclusions, precipitates, and defects in steel [8,9].

The existence of nonmetallic inclusions (irregular shape Al_2O_3 inclusions, high-chemical-activity CaS and MnS inclusions, silicon-rich inclusions, and large-sized carbonitride inclusions) in steel destroy the continuity of the steel matrix and reduce the quality of steel. Inclusions in steel are inevitable byproducts of the deoxidation process of steel making, which are not welcomed by researchers and steelworkers [8,10]. The high elastic modulus of nonmetallic inclusions causes the residual stress of the steel matrix to increase, and obvious stress concentration is formed around the inclusion tip angle or convex boundary, resulting in the formation of microcracks at the matrix/inclusion interface during rolls. These microcracks may be used as pitting part of low-alloy steel [11,12] in corrosive medium environments. Nonmetallic inclusions in steel have been proved to play a negative role in local corrosion. At the same time, CaS and MnS inclusions with high chemical activity are easily dissolved in a corrosive medium to form pits. Many researchers have conducted a lot of work to study the mechanisms of pits caused by inclusions [13–15]. Silicon-rich inclusions are hard and fragile and are incompatible with the steel matrix; therefore, microvoids are formed at the interface of inclusions/steel matrix, and hydrogen is easy to aggregate in these microvoids, leading to hydrogen-induced cracks [16–19]. In recent years, researchers have studied the influence of the number distribution and density of nonmetallic inclusions on local corrosion and the addition of different alloying elements to improve the corrosion resistance of steel. Reformatskaya et al. [20] found that the corrosion rates increased regularly with the increase in the total density of corrosive nonmetallic inclusions, which was not related to the properties of nonmetallic inclusions, as shown in Figure 1.

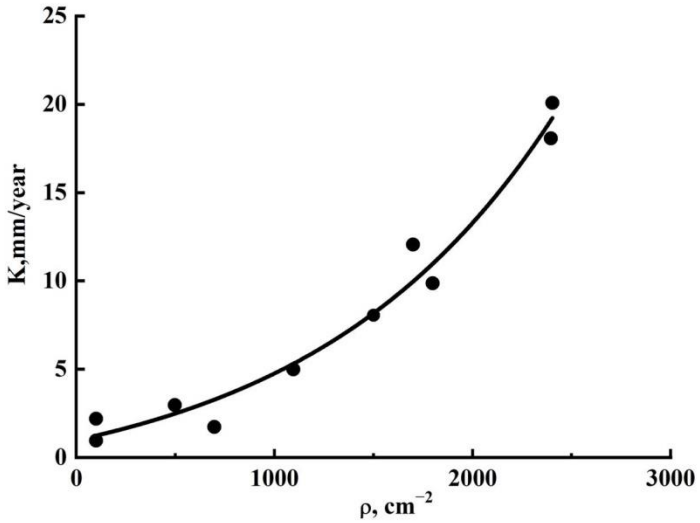


Figure 1. Relationship between corrosion rate and density of corrosive nonmetallic inclusion [20]. Reproduced with permission of Springer, copyright 2022.

In recent decades, Nb, V, and Ti have been widely developed and applied in high-strength, low-alloy steels as important microalloying elements, where nanosized nitrides or carbides precipitate by refining alloy steel grains [21], improving the homogeneity of microstructures, increasing the proportion of low-angle grain boundaries, generating dense, dark, black corrosion products, and improving the corrosion resistance of rebars.

In addition, rare earth elements have attracted more and more attention from iron and steel enterprises because of their strong affinity for sulfur and oxygen. Many studies have shown that rare earth elements in steel can not only purify molten steel, but also modify inclusions, play the role of microalloying elements, and have a positive impact on delaying the corrosion of concrete steel bars [22,23]. This paper systematically presents the role of the inclusion and precipitate phases in inducing steel corrosion globally and provides a theoretical basis for recent research on the corrosion mechanism of rebars under carbonization conditions.

2. The Role of Second-Phase Particles in Corrosion

2.1. The Role of Aluminum Oxides in Corrosion

2.1.1. The Role of Al_2O_3 Inclusions in Corrosion

The nonmetallic inclusions in steel destroy the continuity of the metal matrix and deteriorate the quality of the steel. In the steel-making process, many aluminum oxides of different sizes are generated [24,25], but Al_2O_3 is one of the most common inclusions. Al_2O_3 inclusions are hard and fragile, and microcracks and stress concentrations form around the inclusions during the applied deformation process [26], which damages the mechanical properties of the steel. Pitting corrosion usually occurs at the location of surface chemical or physical unevenness, such as inclusions, precipitates, and defects in the steel [27–32]. Inclusions in steel have been proved to play an important role in localized corrosion. Alumina-containing inclusions are hard, fragile, and incompatible with the steel matrix [15,33]. As a result, microvoids are formed at the inclusion/steel matrix interface, which are permanent traps for hydrogen and can lead to hydrogen-induced cracks [34–36], which become the origin of pitting corrosion and cause steel corrosion.

The shape of Al_2O_3 in steel is irregular, and there are regions of stress concentration and high dislocation density at the sharp corners or raised boundaries of the inclusions, as shown in Figure 2. At the same time, alumina inclusions have higher local impedance [36], which is more stable than the adjacent steel matrix, and preferential dissolution occurs on the steel matrix, while the preferential dissolution is caused by the microcracks at the interface between the Al_2O_3 inclusions and the matrix and the lattice distortion around the inclusions [13,37].

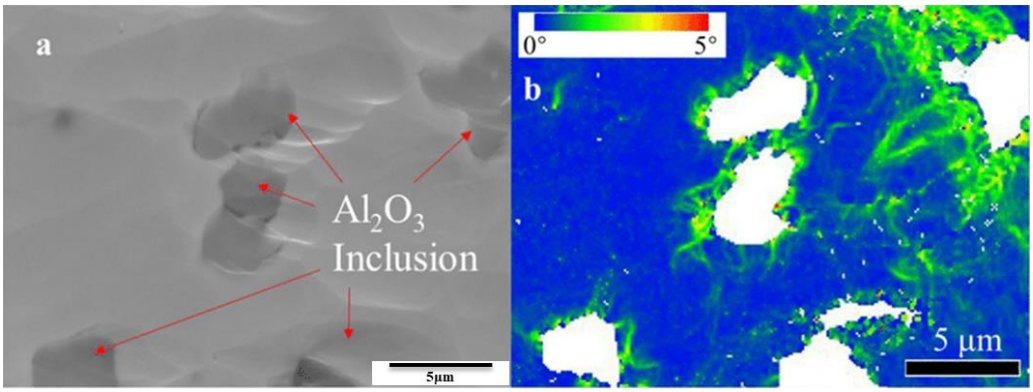


Figure 2. SEM image and KAM image of Al_2O_3 inclusion region. (**a**) FE-SEM image; (**b**) KAM image of the same region as shown in (**a**) [13]. Reproduced with permission of Elsevier, copyright 2018.

From the results of atomic force microscopy (CSAFM, Bruker, Germany), it is found that the conductivity of Al_2O_3 inclusions is worse, as shown in Figure 3, so there is not existed galvanic couple between the Al_2O_3 inclusions and the surrounding steel matrix, so the galvanic corrosion of the Al_2O_3 inclusions and the matrix will not occur. However, crevice corrosion and stress corrosion occurred at the Al_2O_3 inclusion/matrix interface, which caused the matrix around the inclusions to almost dissolve, and Cl^- will accumulate in the pits formed by the dissolution of the matrix, thereby forming a concentration cell, which further accelerates the dissolution of the matrix in the pits [38]. Under the same

corrosion conditions, the local corrosion rate of Al_2O_3 inclusions is mainly affected by its size and components, the radius of the nearly circular corrosion area around the inclusions is significantly different, while its shape and distribution in the steel matrix almost no effect on the corrosion rate [39,40].

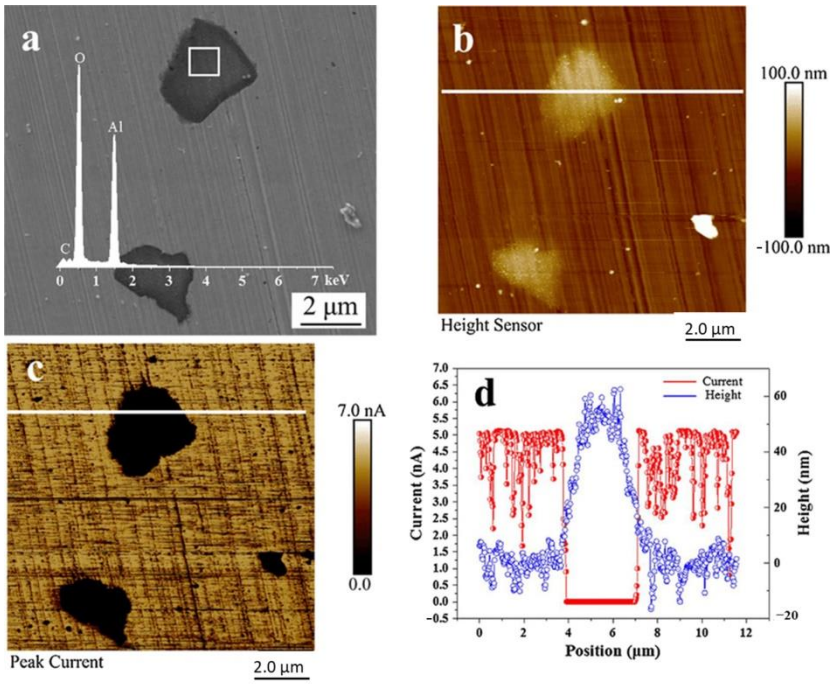


Figure 3. (**a**) SEM and EDS results of inclusions; (**b**) AFM terrain of the same area as (**a**); (**c**) conductivity map of the same area as (**a**); (**d**) line scan analysis results in (**b**,**c**) [13]. Reproduced with permission of Elsevier, copyright 2018.

Villavicencio et al. [40] studied the effect of nonmetallic Al_2O_3 inclusions on the corrosion resistance of API 5L X42 steel under the conditions of neutral solution and found that the number of Al_2O_3 inclusions in the steel matrix was obviously decreased after heat treatment, but it had no effect on the corrosion rate, only promoting pitting corrosion. Jin et al. [16,41] pointed out that Al_2O_3 has a negative effect on hydrogen-induced cracking of pipeline steel. Liu et al. [42] reported that, in the marine environment, pitting corrosion primarily occurred around Al_2O_3 inclusions. Cheng et al. [36] pointed out that the Al_2O_3-rich inclusions are more stable than the adjacent matrix, so the dissolution priority occurs in the steel matrix around the Al_2O_3 inclusions. Some researchers have found [3,13,39,43] that galvanic corrosion cannot occur between Al_2O_3 inclusions and the adjacent steel matrix, but the aggregation of chloride ions and the difference in oxygen concentration in the pits around Al_2O_3 inclusions accelerated the pit expansion.

Due to the high interfacial energy of Al_2O_3 inclusions, the inclusions in liquid steel can easily aggregate into inclusion clusters through collision and coalescence. When the steel matrix around the Al_2O_3 inclusions dissolves to form pits, the stress is mainly concentrated on the edge of the corrosion pits, and the pits develop primarily along the direction parallel to the steel substrate. In the process of pit expansion, the interaction of Al_2O_3 inclusion clusters accelerates the dissolution of the steel matrix between adjacent inclusions and has a greater negative influence on the local corrosion of the steel matrix, as shown in Figure 4. Liu et al. [13] showed that due to the interaction and enhanced the effect of Al_2O_3 inclusion clusters, the steel matrix around the inclusion clusters is more severely dissolved than the matrix around a single inclusion. Liu et al. [44] found that agglomerated Al_2O_3 inclusions had a more negative impact on localized corrosion than isolated Al_2O_3 inclusions.

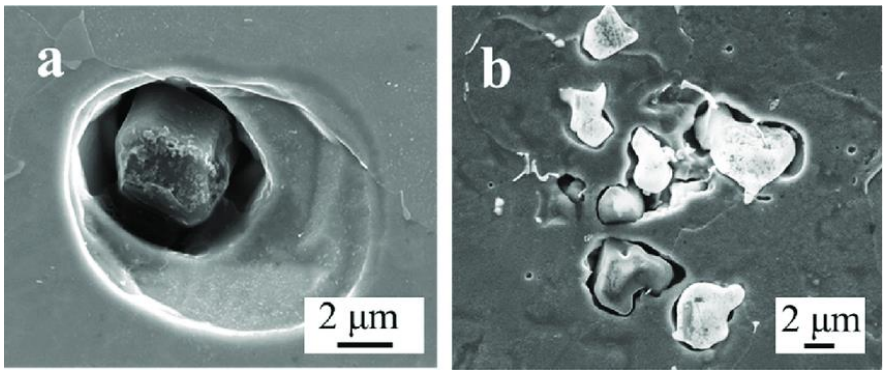


Figure 4. FE-SEM image of pits in steel. (**a**) The morphology of the pit around a single Al_2O_3 inclusion; (**b**) the pit morphology of the Al_2O_3 inclusion cluster [13]. Reproduced with permission of Elsevier, copyright 2018.

2.1.2. Effect of Rare-Earth-Modified Al_2O_3 Inclusions in Corrosion

In recent decades, rare earth elements have received increasing attention from iron and steel enterprises due to their strong affinity for sulfur and oxygen. Some research has shown that the addition of rare earth elements to steel can modify Al_2O_3 inclusions [45] and can also soften high-hardness inclusions by forming $(RE)_2O_2S$ and $(RE)AlO_3$ and reduce the lattice distortion caused by inclusions [46], improving the pitting corrosion resistance of steel [47].

Rare earth has a strong affinity for sulfur and oxygen, and it is easy to form rare earth oxysulfide. The size of inclusions containing rare earth oxysulfide is much smaller than that of normal inclusions [48,49] and usually has a spherical shape (as shown in Figure 5a), and its size is mainly 1–2 μm. So, the rare-earth-modified inclusions still have a greater risk of pitting corrosion. The formation of rare earth oxysulfide changes the morphology of Al_2O_3 inclusions, making the Al_2O_3 inclusions spheroidized into precipitation nuclei, forming $(RE)AlO_3$ in steel [50,51]. As shown in Figure 5, there are two main types of inclusions in RE-added low-carbon steels [52]. The analysis of scanning Kelvin prove force microscopy (SKPFM) results shows that rare-earth-modified inclusions have a much lower electrode potential than the steel matrix [53–55], and the inclusions in the experimental steel are more likely to act as anode phases in the condition containing a corrosive medium. Although the addition of rare-earth-element-modified Al_2O_3 inclusions to steel still has a risk of pitting corrosion, it has a positive effect on protecting the steel matrix and postponing the corrosion rate of the matrix, as shown in Table 1.

Table 1. Corrosion rate variation of steel with corrosion time [45]. Q235: 0.0 wt.% RE; 0.0 wt.% Cu. $0^{\#}$: 0.00 wt.% RE; 0.31 wt.% Cu. $1^{\#}$: 0.0065 wt.% RE; 0.31 wt.% Cu. $2^{\#}$: 0.0089 wt.% RE; 0.30 wt.% Cu. $5^{\#}$: 0.0160 wt.% RE; 0.31 wt.% Cu. $6^{\#}$: 0.021 wt.% RE; 0.31 wt.% Cu. Reproduced with permission of Elsevier, copyright 2010.

Corrosion Time/h	Corrosion Rate of Different Steel Samples					
	Q235	$0^{\#}$	$1^{\#}$	$2^{\#}$	$5^{\#}$	$6^{\#}$
70	5.47	3.30	2.87	3.09	3.00	2.74
140	3.90	2.56	2.26	2.26	2.24	2.21
240	3.31	2.21	2.02	1.89	1.76	1.88

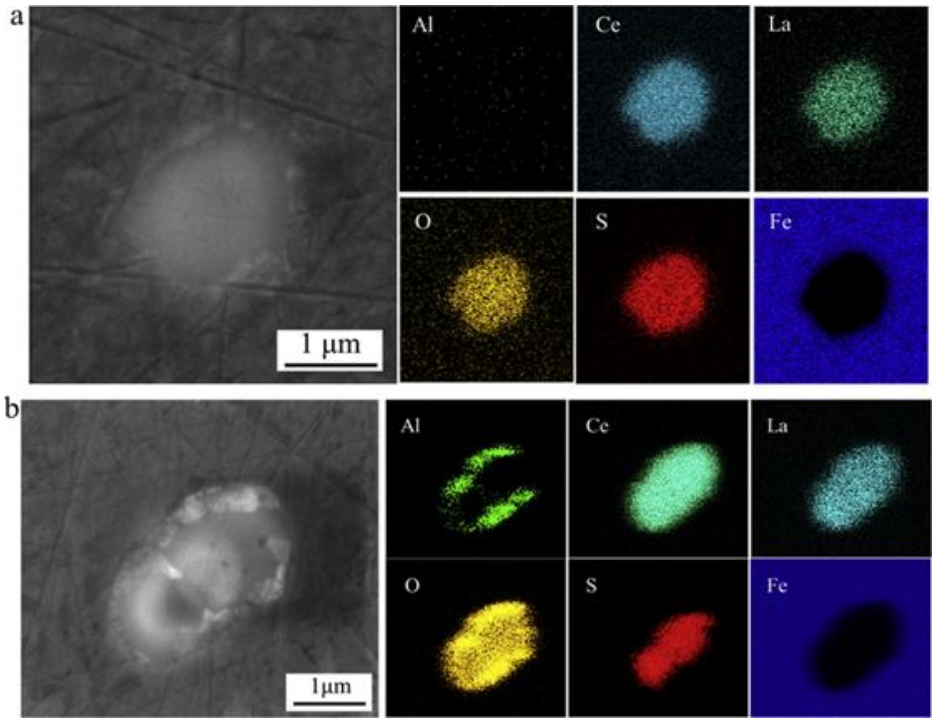


Figure 5. SEM-EDS images of inclusions in the sample steel. (**a**) Morphology and elemental distribution of (RE)2O2S-(RE)xSy; (**b**) morphology and elemental distribution of (RE)AlO3-(RE)2O2S-(RE)xSy [52]. Reproduced with permission of Elsevier, copyright 2017.

Liu et al. [37] studied the effect of rare earth metals on the local corrosion induced by Al_2O_3 inclusions in Zr-Ti-deoxidized steel and found that the induced and extended mechanisms of local corrosion were completely different before and after adding rare earth. Localized corrosion of Zr-Ti-deoxidized steel begins with microcracks/lattice distortion around ZrO_2-Ti_2O_3-Al_2O_3 inclusions. After the addition of rare earth, the dissolution of $(RE)_2O_2S$-(RE)xSy caused local corrosion, and the acidic corrosion medium in the micropits aggregated, which promoted the extension of the micropits. Some researchers have pointed out [51,56,57] that Al_2O_3 inclusions are one of the main sources of pit nucleation sites, the metastable pit life is directly related to the size of the inclusions, and inclusions smaller than 1 μm are rarely transformed into steady-state pits. Therefore, effectively controlling the size and quantity of inclusions in steel may be a feasible way to improve the corrosion resistance of steel.

2.2. The Role of Carbonitride Precipitates in Corrosion

2.2.1. The Role of Carbide Precipitation in Corrosion

Studies have shown that carbide precipitation as cathode hydrogen evolution and hydrogen oxidation in steel reduces the activation energy of metal, reduces the pH of the corrosion medium, accelerates anodic dissolution, and induces crevice corrosion through the hydrogen-induced cracking mechanism. The nanosized carbide precipitates can refine the alloy steel grains, improve the uniformity of the microstructure, increase the proportion of small-angle grain boundaries, and improve the corrosion resistance of the steel matrix.

Zhao et al. [58] showed that nano-NbC precipitates are regarded as cathodes for galvanic corrosion but have little effect on the macroscopic corrosion behavior of high strength low alloy (HSLA) steel in simulated seawater, while the microstructure has a more significant effect on corrosion than nano-carbide precipitates. Some researchers [56,57] consider that precipitates with phase size much smaller than 1 μm are either harmless or basically beneficial to corrosion.

On the other hand, nano-carbide precipitation can be regarded as an effective hydrogen trap to capture a certain amount of hydrogen, prevent the diffusion and aggregation of hydrogen, and improve the corrosion resistance of steel. Studies have shown [59–62] that hydrogen accelerates anodic dissolution and hinders the transformation of steel from active dissolution to passivating, while nanosized NbC precipitation can effectively capture hydrogen, hindering the diffusion and aggregation of hydrogen in steel, and improve the corrosion resistance of steel. Li et al. [4] studied the different effects of nano-NbC precipitation on the corrosion behavior of HSLA steel and found that, in the non-hydrogen steel, the effect of the NbC precipitation phase was almost negligible, while in the hydrogen-containing steel, the NbC precipitation phase significantly improved corrosion resistance of the steel.

At the same time, the corrosion products of Nb-containing steel are tighter than those without Nb, and have better bonding performance with the matrix, which can hinder the migration of corrosion ions and improve the corrosion resistance of steel. Wang et al. [63] found that the rust layers resistance of bainitic weathering steel is higher, and the rust layer has better tightness, a better ability to hinder ion penetration, and has better corrosion resistance. Guo et al. [64] show that the corrosion resistance of the low-alloy steel rust layer depends on the tightness of the rust layer and the bonding properties of the rust base, rather than the rust phase formed in the initial period of corrosion. Wang et al. [65] found that the inner black corrosion product of steel containing a certain amount of Nb is tighter than the corrosion product of non-Nb steel, which hinders the migration of corrosion ions to a certain extent and postpones the corrosion of the internal matrix.

2.2.2. The Role of Nitride Precipitation in Corrosion

The microcracks generated by the intrusion of hydrogen generated by the corrosion of steel in corrosive media, and the high dislocation density region around the inclusions are usually easily induced by pitting corrosion. The highly dispersed nitride precipitates can improve the pitting-corrosion-induced and hydrogen-induced cracks and dislocations to a certain extent.

With the addition of Nb, the precipitation of the precipitated phase at the grain boundary has a significant hindering effect on the movement of dislocations, as shown in Figure 6, which leads to the increase in local dislocation density and promotes the progress of local corrosion. On the other hand, the number of low-angle grain boundaries in the structure is increased, which effectively improves the corrosion resistance of grain boundaries. Under the combined effect of the above-mentioned microstructures, the corrosion rate of steel shows a law of first decreasing and then increasing with the increase in Nb content. At the same time, as an effective hydrogen trap, the nitride precipitation can adsorb a certain amount of hydrogen, which significantly improves the resistance to hydrogen-activated corrosion.

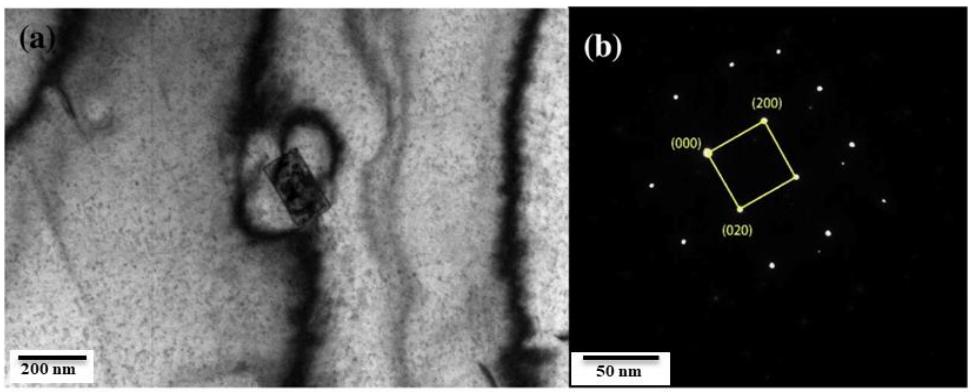


Figure 6. (**a**) TEM morphology of the precipitated phase; (**b**) SAED mode of the precipitated phase [66]. Reproduced with permission of Elsevier, copyright 2020.

Li et al. [4] found that the corrosion resistance of Nb-containing steel is higher than that of non-Nb steel. Wang et al. [65] show that adding a certain amount of Nb can improve the uniformity of X80 steel and increase the proportion of low angle grain boundaries, thereby improving the corrosion resistance of X80 steel. Yue et al. [67] found that with the continuous increase in Nb content, the local dislocation density increased, and the advantages of low angle grain boundaries were less than the disadvantages of local dislocations, that is, the corrosion resistance of the steel plate decreased.

Since the precipitated phase and the matrix are in intimate contact, there is no gap between them (Figure 7), so crevice corrosion does not occur. However, the (Nb, V, Ti) N precipitate and the iron matrix have good electrical conductivity, so a corrosion galvanic couple can be formed between them, the precipitate acts as the cathode, and the matrix acts as the anode. In the corrosive medium, the precipitation phase and the matrix form galvanic corrosion to produce small and shallow pits, and some corrosion products are covered on the pits, which delays the further corrosion caused by the aggregation of corrosion ions in the pits. In addition, there are two combinations of inclusions and nitride precipitates: (1) the inclusions are completely surrounded by the nitride precipitation phase, the rate of initiation and expansion of pitting corrosion is low, and the combined inclusions and the matrix around the precipitate gradually dissolve to form pits; (2) the inclusions are not completely encapsulated by the nitride precipitates, and due to the combination of the inclusions and the precipitates leading to a faster corrosion initiation rate, the inclusions dissolve to form pits.

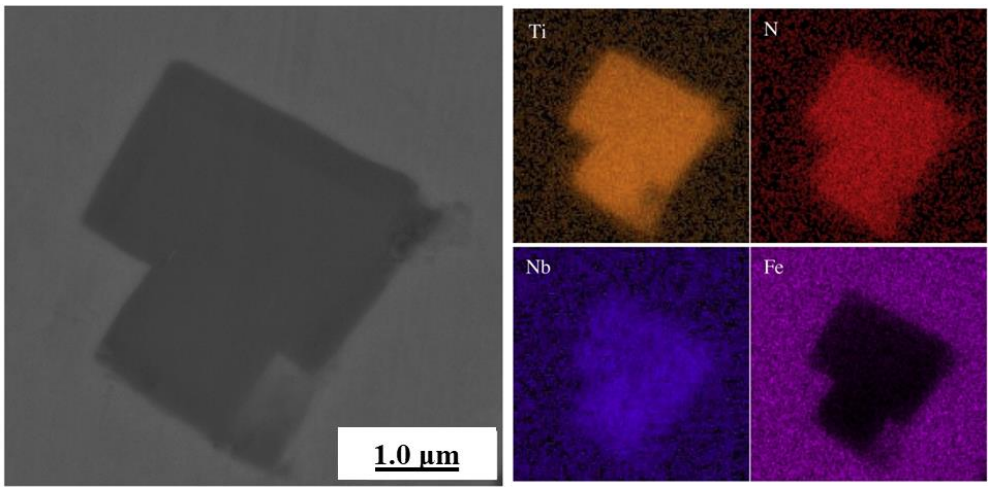


Figure 7. Morphology and element distribution of (Ti, Nb) N precipitation in Sb-containing weathering steel [66]. Reproduced with permission of Elsevier, copyright 2020.

Xue et al. [66] found that (Ti, Nb) N precipitates formed a galvanic couple with the matrix to form unstable small and shallow pits, which reduced the rate of pitting initiation and expansion to a certain extent. Wallaert et al. [62] show that NbN precipitation can act as a hydrogen trap, and capture hydrogen near grain boundaries, thereby improving the corrosion resistance of steel.

2.3. The Role of Sulfide Inclusions in Corrosion

There are few types of sulfide inclusions and cannot be directly generated in molten steel, but sulfide inclusions are precipitated between dendrites due to the segregation of sulfur when molten steel solidifies. The size and quantity of precipitated sulfide particles are mainly affected by the cooling rate of molten steel [29]. Sulfur-containing inclusions have high electrochemical activity and easily become the starting point of steel corrosion in a near-neutral pH marine environment, while the sulfide inclusions that cause pitting corrosion are mainly CaS and MnS inclusions.

2.3.1. The Role of CaS Inclusions in Corrosion

The high probability of formation of CaS inclusions in low-alloy and -carbon steels is caused by the low solubility of calcium, the formed CaS has a sufficiently high electrochemical activity in the corrosive medium, which leads to the preferential dissolution of the coarse CaS inclusions in the steel matrix, and the H_2S generated by the dissolution is enriched in the voids formed by the dissolution of the inclusions, making the void solution more acidic, thereby further promoting corrosion of inclusions. At the same time, microcracks exist at the interface between the CaS inclusions with higher thermal expansion coefficients and the steel matrix, which are also a sensitive position for localized corrosion.

For CaS-containing Ds-type inclusions, the initiation and expansion processes of corrosion are quite different and can be divided into three stages, as shown in Figure 8. In the first stage, corrosion occurs preferentially at the CaS/steel matrix interface due to microcracks and electrochemical inhomogeneity. The dissolution of CaS and the steel matrix generates acidic ions such as HS^- and H^+, which increase the acidity of the interstitial solution at the CaS/steel matrix interface, resulting in an accelerated electrochemical dissolution rate of the steel matrix (Figure 8a). In the second stage, the CaS inclusions are completely dissolved, and the chemical dissolution of xAl_2O_3-yCaO dominates the corrosion process. The CaS inclusions were completely dissolved, and thus the protected region started to be destroyed, resulting in a reduction in diameter and localized attack in this region (Figure 8b). The third stage is until the xAl_2O_3-yCaO is completely dissolved and the MgO-Al_2O_3 inclusions fall off (Figure 8c).

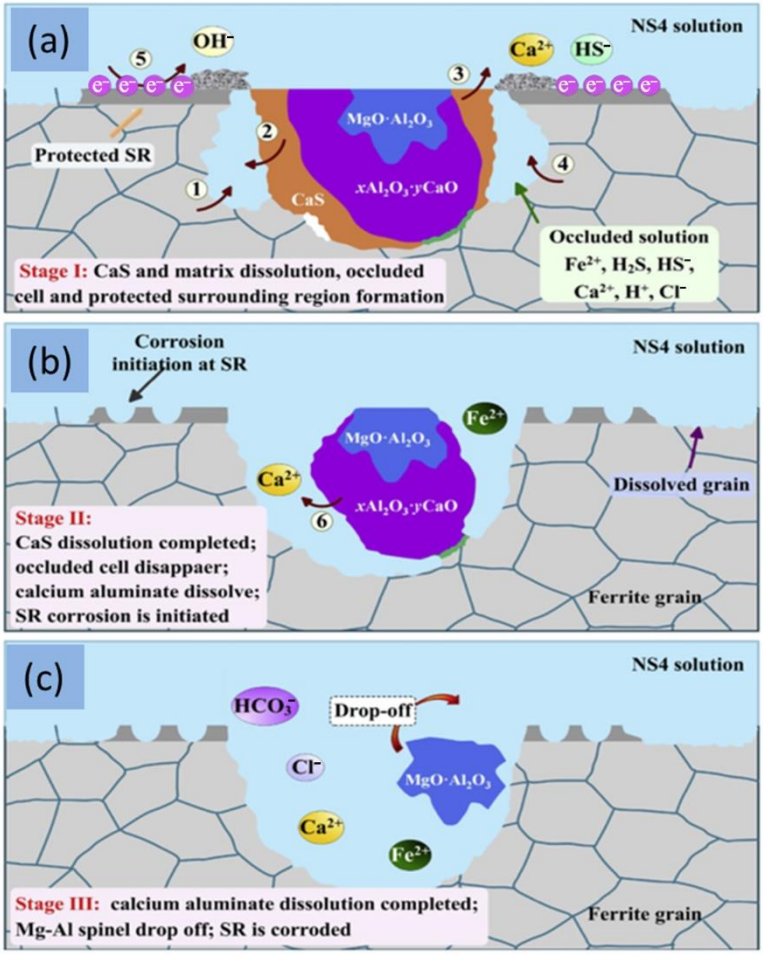


Figure 8. Schematic diagram of pit initiation and expansion process around Ds−type inclusions. (**a**) at stage I, (**b**) at stage II, (**c**) at stage III [11]. Reproduced with permission of Elsevier, copyright 2019.

Some researchers [9,12,68] found that inclusions containing CaS were the most corrosive and had the fastest dissolution rate in electrolyte solutions. Wang et al. [12] showed that the dissolution of CaS in Ds-type inclusions is produced an acidic environment, which promotes crevice corrosion between the inclusions and the matrix; the occluded space between the inside and outside of the void leads to the formation of a protected region around the inclusions, which gradually disappears until the CaS inclusions are completely dissolved. Reformatskaya et al. [20] show that the composite inclusions with calcium aluminate as the core and surrounded by CaS are more prone to corrosion than MnS inclusions.

2.3.2. The Role of MnS Inclusions in Corrosion

Under the condition of Cl^- and near-neutral pH, the nonmetallic inclusion MnS is a good precursor and a pitting-sensitive point for pitting corrosion of rebars [69,70], and its ability to induce pitting corrosion depends on the size and shape of the inclusions. MnS inclusions with a size less than 0.7 μm in steel failed to form corrosion pits. The first step leading to pit germination is the easy dissolution of the MnS inclusions, and the adsorption of their released sulfides into the surrounding passivation film, which initiates electrochemical corrosion at the inclusion/matrix interface. Due to the strong influence of sulfide adsorption on the matrix after the chemical dissolution of the inclusions, the passivation region around the inclusions is almost destroyed, while the sulfide-rich grains far from the inclusions show larger passivation region, and the electrochemical dissolution of MnS inclusions is catalyzed by chlorides in solution. Unlike stainless steels, in carbon and microalloyed steels, the iron matrix around some MnS inclusions is more anodic than the inclusion-free iron matrix due to the effect of interdendritic residual stress and microcracks around the edges of the inclusions. In Cl^--containing solutions, it is believed that chloride ions tend to accumulate at the carbon steel inclusion/matrix interface to the initiate catalytic pitting corrosion, resulting in the anodic dissolution of the matrix at locations susceptible to pit corrosion.

Williams et al. [71] believed that the preferential dissolution of highly chemically active, sulfide-rich circles around MnS inclusions was responsible for the initiation of pitting corrosion. Avci et al. [72] showed that MnS inclusions on 1080 carbon steel did not dissolve in the initial stage of pitting corrosion. Alkire et al. [73,74] proved that corrosion pits will not initiate at MnS inclusions smaller than 0.7 μm. Park et al. [75] found that initial pits appeared at the MnS particles of complex inclusions in transformation induced plasticit (TRIP) steel, initial pits were formed at the Mn-oxysulfide particles of complex inclusions in twinning induced plasticity (TWIP) steel, and the dual-phase (DP) steel forms initial pits on the metal matrix around the interface between the single MnS inclusion and the matrix. Zhou et al. [76] found that the surface of dislocations with edge and spiral characteristics is the preferred position for MnS dissolution. Wei et al. [77] found that the galvanic couple between the MnS inclusions and the steel matrix in ultra-low-carbon steel was the cause of the initial formation of early localized corrosion. Negheimish et al. [78] found that the corrosion rates of MnS inclusion-containing steel (abbreviated as IS) was about twice that of normal steel (abbreviated as NS, without MnS inclusions) in simulated concrete pore solutions with different pH values, as shown in Figure 9.

In summary, the role of the second-phase particles in inducing corrosion of rebars is summarized, as shown in Table 2.

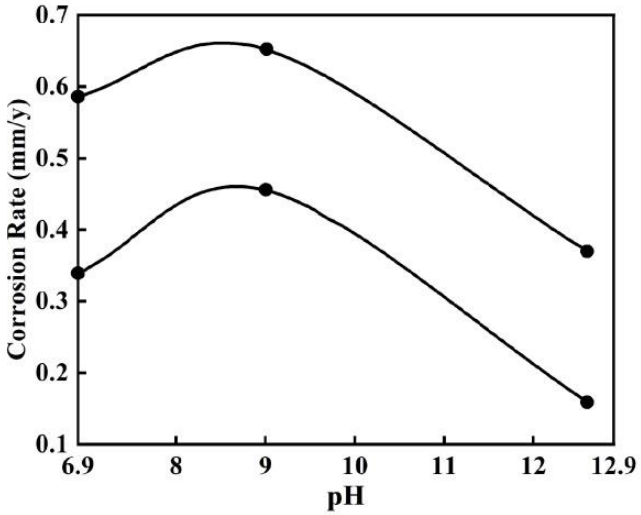


Figure 9. Corrosion rates of IS and NS rebars in different pH solutions [78]. Reproduced with permission of National Association of Corrosion Engineers, copyright 2022.

Table 2. The role of second phase particles in inducing corrosion of rebars.

Second-Phase Particles	Can a Galvanic Couple Be Formed?	Corrosive Behavior	Anode or Cathode	Preferential Dissolution Region	Remark	Reference
Al_2O_3	No	Crevice corrosion, Stress corrosion	\	Interface between inclusion and matrix	1. The interaction of Al_2O_3 inclusion clusters accelerates the dissolution of the surrounding steel matrix; 2. Al_2O_3 inclusion clusters have a more negative impact on localized corrosion than single inclusions.	[13,15,16,21,27,28,37,39]
Rare earth modified Al_2O_3	No	Pitting corrosion	Anode	$(RE)_2O_2S$-(RE)xSy	Adding (RE) elements can modify Al_2O_3 inclusions, effectively control the size, shape, and quantity of Al_2O_3 inclusions, and improve the corrosion resistance of steel.	[45,48,50–53]
Carbide	Yes	Galvanic corrosion	Cathode	Steel matrix	Adding an appropriate amount of Nb, V, Ti can: 1. Refine the grains of alloy steel and improve the uniformity of microstructure; 2. Increase the proportion of low-angle grain boundaries; 3. Hinder the diffusion and aggregation of hydrogen; 4. Generate dark black dense rust layer; improve the corrosion resistance of steel.	[58–60,65]
Nitride	Yes	Galvanic corrosion	Cathode	Steel matrix		[4,65–67]
CaS	No	Pitting corrosion	Anode	CaS inclusion	CaS dissolves preferentially, lowering the pH of the pore solution and further promoting corrosion.	[9,12,20,68]
MnS	No	Pitting corrosion	Anode	MnS inclusion	1. Corrosion damage around the passivation region; 2. Electrochemical dissolution occurs to form pits.	[71,72,75–77]

3. Conclusions

(1) At present, there are three main ways of local corrosion of microalloyed high-strength rebars caused by second-phase particles: pitting corrosion, crevice corrosion, and stress corrosion.

(2) The research progressed on corrosion induced by Al_2O_3, (RE)-AlO_3, CaS, MnS, carbonitride, and other second phase particles in microalloyed high-strength rebars is

mainly expounded. The current research shows that sulfide inclusions are harmful to the corrosion resistance of microalloyed, high-strength rebars, and different characteristics of Al_2O_3 inclusions have different effects on the corrosion resistance of rebars. For this phenomenon, many researchers add alloying elements and rare earth elements to steel to modify inclusions, refine grains, and improve microstructures, so as to improve the corrosion resistance of microalloyed, high-strength rebars.

(3) At present, the main shortcomings of the research on the corrosion induced by the second phase particles are that the researchers start from a single inclusion and the microscopic angle, and the lack of research on the relationship between the number, density, and distribution of inclusions in steel bars and the corrosion resistance of microalloyed, high-strength steel bars.

Author Contributions: Conceptualization, S.L. and C.L.; methodology, S.L., Z.Z., S.H. and J.Y.; formal analysis, S.L., C.Z. and C.L.; writing—original draft preparation, S.L. and C.L.; writing—review and editing, S.L., C.Z. and C.L.; funding acquisition, C.L. All authors have read and agreed to the published version of the manuscript.

Funding: This project is s financially supported by the National Science Foundation of China with the grant No. 52074095, 52164032.

Institutional Review Board Statement: Not applicable.

Informed Consent Statement: Not applicable.

Data Availability Statement: The data used to support the findings of this study are available from the corresponding authors upon reasonable request.

Conflicts of Interest: The authors declare no conflict of interest.

References

1. Liu, S.; Sun, C.; Niu, D. A review of research on critical chloride ion concentration for steel corrosion. *Silic. Bull.* **2014**, *33*, 83–91. [CrossRef]
2. Li, J.; Xiong, J.; Fan, Z.; Zheng, H.; Li, W. Research progress and prospect of macro cell corrosion of rebars in concrete. *J. Silic.* **2021**, *49*, 11. [CrossRef]
3. Yang, Y.; Zhang, T.; Shao, Y.; Meng, G.; Wang, F. New understanding of the effect of hydrostatic pressure on the corrosion of Ni–Cr–Mo–V high strength steel. *Corros. Sci.* **2013**, *73*, 250–261. [CrossRef]
4. Li, J.; Wu, J.; Wang, Z.; Zhang, S.; Wu, X.; Huang, Y.; Li, X. The effect of nanosized NbC precipitates on electrochemical corrosion behavior of high-strength low-alloy steel in 3.5% NaCl solution. *Int. J. Hydrogen Energy* **2017**, *42*, 22175–22184. [CrossRef]
5. Wang, L.; Tian, H.; Gao, H.; Xie, F.; Zhao, K.; Cui, Z. Electrochemical and XPS analytical investigation of the accelerative effect of bicarbonate/carbonate ions on AISI 304 in alkaline environment. *Appl. Surf. Sci.* **2019**, *492*, 792–807. [CrossRef]
6. Hou, B.; Li, X.; Ma, X.; Du, C.; Zhang, D.; Zheng, M.; Xu, W.; Lu, D.; Ma, F. The cost of corrosion in China. *NPJ Mater. Degrad.* **2017**, *1*, 4. [CrossRef]
7. Li, X.; Zhang, D.; Liu, Z.; Li, Z.; Du, C.; Dong, C. Materials science: Share corrosion data. *Nature* **2015**, *527*, 441–442. [CrossRef]
8. Lind, M.; Holappa, L. Transformation of Alumina Inclusions by Calcium Treatment. *Met. Mater. Trans. A* **2010**, *41*, 359–366. [CrossRef]
9. Verma, N.; Pistorius, P.C.; Fruehan, R.J.; Potter, M.; Lind, M.; Story, S.R. Transient inclusion evolution during modification of alumina inclusions by calcium in liquid steel: Part I. Background, Ex-perimental Techniques and Analysis Methods. *Met. Mater. Trans. B* **2011**, *42*, 711–719. [CrossRef]
10. Opiela, M.; Grajcar, A. Modification of Non-Metallic Inclusions by Rare-Earth Elements in Microalloyed Steels. *Arch. Foundry Eng.* **2012**, *12*, 129–134. [CrossRef]
11. Wang, L.; Xin, J.; Cheng, L.; Zhao, K.; Sun, B.; Li, J.; Wang, X.; Cui, Z. Influence of inclusions on initiation of pitting corrosion and stress corrosion cracking of X70 steel in near-neutral pH environment. *Corros. Sci.* **2019**, *147*, 108–127. [CrossRef]
12. Liu, C.; Revilla, R.I.; Zhang, D.; Liu, Z.; Lutz, A.; Zhang, F.; Zhao, T.; Ma, H.; Li, X.; Terryn, H. Role of Al2O3 inclusions on the localized corrosion of Q460NH weathering steel in marine environment. *Corros. Sci.* **2018**, *138*, 96–104. [CrossRef]
13. . Szklarska-Śmialowska, Z.; Lunarska, E. The effect of sulfide inclusions on the susceptibility of steels to pitting, stress corrosion cracking and hydrogen embrittlement. *Mater. Corros.* **1981**, *32*, 478–485. [CrossRef]
14. Ha, H.; Park, C.; Kwon, H. Effects of misch metal on the formation of non-metallic inclusions and the associated resistance to pitting corrosion in 25% Cr duplex stainless steels. *Scr. Mater.* **2006**, *55*, 991–994. [CrossRef]
15. Punckt, C.; Boelscher, M.; Rotermund, H.H.; Mikhailov, A.S.; Organ, L.; Budiansky, N.; Scully, J.R.; Hudson, J.L. Sudden Onset of Pitting Corrosion on Stainless Steel as a Critical Phenomenon. *ChemInform* **2004**, *305*, 1133–1136. [CrossRef]

16. da Costa-Mattos, H.; Bastos, I.; Gomes, J. A simple model for slow strain rate and constant load corrosion tests of austenitic stainless steel in acid aqueous solution containing sodium chloride. *Corros. Sci.* **2008**, *50*, 2858–2866. [CrossRef]
17. Liu, Z.; Li, X.; Du, C.; Lu, L.; Zhang, Y.; Cheng, Y. Effect of inclusions on initiation of stress corrosion cracks in X70 pipeline steel in an acidic soil environment. *Corros. Sci.* **2009**, *51*, 895–900. [CrossRef]
18. Jin, T.; Liu, Z.; Cheng, Y. Effect of non-metallic inclusions on hydrogen-induced cracking of API5L X100 steel. *Int. J. Hydrogen Energy* **2010**, *35*, 8014–8021. [CrossRef]
19. Gu, B.; Yu, W.Z.; Luo, J.L.; Mao, X. Transgranular Stress Corrosion Cracking of X-80 and X-52 Pipeline Steels in Dilute Aqueous Solution with Near-Neutral pH. *Corrosion* **1999**, *55*, 312–318. [CrossRef]
20. Reformatskaya, I.I.; Rodionova, I.G.; Beilin, Y.A.; Nisel'Son, L.A.; Podobaev, A.N. The Effect of Nonmetal Inclusions and Microstructure on Local Corrosion of Carbon and Low-alloyed Steels. *Prot. Met.* **2004**, *40*, 447–452. [CrossRef]
21. Xie, Z.; Ma, X.; Shang, C.; Wang, X.; Subramanian, S. Nano-sized precipitation and properties of a low carbon niobium micro-alloyed bainitic steel. *Mater. Sci. Eng. A* **2015**, *641*, 37–44. [CrossRef]
22. Wang, L.; Lin, Q.; Ji, J.; Lan, D. New study concerning development of application of rare earth metals in steels. *J. Alloys Compd.* **2006**, *408–412*, 384–386. [CrossRef]
23. Wilson, W.G.; Kay, D.A.R.; Vahed, A. The use of thermodynamics and phase equilibria to predict the behavior of the rare earth elements in steel. *JOM* **1974**, *26*, 14–23. [CrossRef]
24. Choi, J.-Y.; Kim, S.-K.; Kang, Y.-B.; Lee, H.-G. Compositional Evolution of Oxide Inclusions in Austenitic Stainless Steel during Continuous Casting. *Steel Res. Int.* **2015**, *86*, 284–292. [CrossRef]
25. Liu, C.; Yang, S.; Li, J.; Ni, H.; Zhang, X. The Influence of FeO on the Reaction between Fe–Al–Ca Alloy and Al2O3–CaO–FeO Oxide during Heat Treatment at 1473 K. *Metals* **2017**, *7*, 129. [CrossRef]
26. Arafin, M.; Szpunar, J. A new understanding of intergranular stress corrosion cracking resistance of pipeline steel through grain boundary character and crystallographic texture studies. *Corros. Sci.* **2009**, *51*, 119–128. [CrossRef]
27. Torkkeli, J.; Saukkonen, T.; Hänninen, H. Effect of MnS inclusion dissolution on carbon steel stress corrosion cracking in fuel-grade ethanol. *Corros. Sci.* **2015**, *96*, 14–22. [CrossRef]
28. Tewary, N.; Kundu, A.; Nandi, R.; Saha, J.; Ghosh, S. Microstructural characterisation and corrosion performance of old railway girder bridge steel and modern weathering structural steel. *Corros. Sci.* **2016**, *113*, 57–63. [CrossRef]
29. Man, C.; Dong, C.; Xiao, K.; Yu, Q.; Li, X. The Combined Effect of Chemical and Structural Factors on Pitting Corrosion Induced by MnS-(Cr, Mn, Al)O Duplex Inclusions. *Corrosion* **2017**, *74*, 312–325. [CrossRef]
30. Shibaeva, T.V.; Laurinavichyute, V.; Tsirlina, G.; Arsenkin, A.M.; Grigorovich, K.V. The effect of microstructure and non-metallic inclusions on corrosion behavior of low carbon steel in chloride containing solutions. *Corros. Sci.* **2014**, *80*, 299–308. [CrossRef]
31. Vignal, V.; Krawiec, H.; Heintz, O.; Oltra, R. The use of local electrochemical probes and surface analysis methods to study the electrochemical behaviour and pitting corrosion of stainless steels. *Electrochimica Acta* **2007**, *52*, 4994–5001. [CrossRef]
32. Krawiec, H.; Vignal, V.; Oltra, R. Use of the electrochemical microcell technique and the SVET for monitoring pitting corrosion at MnS inclusions. *Electrochem. Commun.* **2004**, *6*, 655–660. [CrossRef]
33. Xue, H.; Cheng, Y. Characterization of inclusions of X80 pipeline steel and its correlation with hydrogen-induced cracking. *Corros. Sci.* **2011**, *53*, 1201–1208. [CrossRef]
34. Krawiec, H.; Vignal, V.; Heintz, O.; Oltra, R. Influence of the dissolution of MnS inclusions under free corrosion and potentiostatic conditions on the composition of passive films and the electrochemical behaviour of stainless steels. *Electrochimica Acta* **2006**, *51*, 3235–3243. [CrossRef]
35. Suter, T.; Webb, E.G.; Böhni, H.; Alkire, R.C. Pit Initiation on Stainless Steels in 1 M NaCl With and Without Mechanical Stress. *J. Electrochem. Soc.* **2001**, *148*, B174–B185. [CrossRef]
36. Jin, T.; Cheng, Y. In situ characterization by localized electrochemical impedance spectroscopy of the electrochemical activity of microscopic inclusions in an X100 steel. *Corros. Sci.* **2011**, *53*, 850–853. [CrossRef]
37. Liu, C.; Jiang, Z.; Zhao, J.; Cheng, X.; Liu, Z.; Zhang, D.; Li, X. Influence of rare earth metals on mechanisms of localised corrosion induced by inclusions in Zr-Ti deoxidised low alloy steel. *Corros. Sci.* **2020**, *166*, 108461–108463. [CrossRef]
38. Brossia, C.S.; Kelly, R.G. Influence of Alloy Sulfur Content and Bulk Electrolyte Composition on Crevice Corrosion Initiation of Austenitic Stainless Steel. *Corrosion* **1998**, *54*, 145–154. [CrossRef]
39. Wei, W.-Z.; Wu, K.-M.; Liu, J.; Cheng, L.; Zhang, X. Initiation and propagation of localized corrosion induced by (Zr, Ti, Al)-Ox inclusions in low-alloy steels in marine environment. *J. Iron Steel Res. Int.* **2020**, *28*, 453–463. [CrossRef]
40. Villavicencio, J.; Ulloa, N.; Lozada, L.; Moreno, M.; Castro, L. The role of non-metallic Al2O3 inclusions, heat treatments and microstructure on the corrosion resistance of an API 5L X42 steel. *J. Mater. Res. Technol.* **2020**, *9*, 5894–5911. [CrossRef]
41. Dong, C.; Liu, Z.; Li, X.; Cheng, Y. Effects of hydrogen-charging on the susceptibility of X100 pipeline steel to hydrogen-induced cracking. *Int. J. Hydrogen Energy* **2009**, *34*, 9879–9884. [CrossRef]
42. Liu, C.; Cheng, X.; Dai, Z.; Liu, R.; Li, Z.; Cui, L.; Chen, M.; Ke, L. Synergistic Effect of Al2O3 Inclusion and Pearlite on the Localized Corrosion Evolution Process of Carbon Steel in Marine Environment. *Materials* **2018**, *11*, 2277. [CrossRef] [PubMed]
43. Zheng, S.; Li, C.; Qi, Y.; Chen, L.; Chen, C. Mechanism of (Mg,Al,Ca)-oxide inclusion-induced pitting corrosion in 316L stainless steel exposed to sulphur environments containing chloride ion. *Corros. Sci.* **2013**, *67*, 20–31. [CrossRef]
44. Liu, Q.; Yang, S.; Zhao, M.; Zhu, L.; Li, J. Pitting Corrosion of Steel Induced by Al2O3 Inclusions. *Metals* **2017**, *7*, 347. [CrossRef]

45. Yue, L.; Wang, L.; Han, J. Effects of rare earth on inclusions and corrosion resistance of 10PCuRE weathering steel. *J. Rare Earths* **2010**, *28*, 952–956. [CrossRef]
46. Hirata, H.; Isobe, K. Steel Having Finely Dispersed Inclusions. U.S. Patemt US10547303[P], 20 July 2006.
47. Kim, S.-T.; Jeon, S.-H.; Lee, I.-S.; Park, Y.-S. Effects of rare earth metals addition on the resistance to pitting corrosion of super duplex stainless steel—Part 1. *Corros. Sci.* **2010**, *52*, 1897–1904. [CrossRef]
48. Jeon, S.-H.; Kim, S.-T.; Choi, M.-S.; Kim, J.-S.; Kim, K.-T.; Park, Y.-S. Effects of cerium on the compositional variations in and around inclusions and the initiation and propagation of pitting corrosion in hyperduplex stainless steels. *Corros. Sci.* **2013**, *75*, 367–375. [CrossRef]
49. Jeon, S.-H.; Kim, S.-T.; Lee, I.-S.; Park, Y.-S. Effects of sulfur addition on pitting corrosion and machinability behavior of super duplex stainless steel containing rare earth metals: Part 2. *Corros. Sci.* **2010**, *52*, 3537–3547. [CrossRef]
50. Adabavazeh, Z.; Hwang, W.S.; Su, Y.H. Effect of Adding Cerium on Microstructure and Morphology of Ce-Based Inclusions Formed in Low-Carbon Steel. *Sci. Rep.* **2017**, *7*, 46503. [CrossRef]
51. Li, N.; Wang, Y.; Qiu, S.; Xiang, L. Effect of Ce on the Evolution of Recrystallization Texture in a 1.2%Si-0.4%Al Non-oriented Electrical Steel. *ISIJ Int.* **2016**, *56*, 1256–1261. [CrossRef]
52. Liu, C.; Revilla, R.I.; Liu, Z.; Zhang, D.; Li, X.; Terryn, H. Effect of inclusions modified by rare earth elements (Ce, La) on localized marine corrosion in Q460NH weathering steel. *Corros. Sci.* **2017**, *129*, 82–90. [CrossRef]
53. Afshar, F.N.; de Wit, J.; Terryn, H.; Mol, J. Scanning Kelvin probe force microscopy as a means of predicting the electrochemical characteristics of the surface of a modified AA4xxx/AA3xxx (Al alloys) brazing sheet. *Electrochimica Acta* **2013**, *88*, 330–339. [CrossRef]
54. Sathirachinda, N.; Pettersson, R.; Wessman, S.; Pan, J. Study of nobility of chromium nitrides in isothermally aged duplex stainless steels by using SKPFM and SEM/EDS. *Corros. Sci.* **2010**, *52*, 179–186. [CrossRef]
55. Williams, D.E.; Zhu, Y.Y. Explanation for Initiation of Pitting Corrosion of Stainless Steels at Sulfide Inclusions. *J. Electrochem. Soc.* **2000**, *147*, 1763–1766. [CrossRef]
56. Suter, T.; Böhni, H. A new microelectrochemical method to study pit initiation on stainless steels. *Electrochimica Acta* **1997**, *42*, 3275–3280. [CrossRef]
57. Stewart, J.; Williams, D.E. The initiation of pitting corrosion on austenitic stainless steel: On the role and importance of sulphide inclusions. *Corros. Sci.* **1992**, *33*, 457–474. [CrossRef]
58. Zhao, Q.; Wang, Z.; Fan, E.; Wu, X.; Huang, Y.; Li, X. Effects of Nanosized Nb Carbide Precipitates on the Corrosion Behavior of High-Strength Low-Alloy Steel in Simulated Seawater. *Int. J. Electrochem. Sci.* **2017**, *12*, 7989–7996. [CrossRef]
59. Zhang, S.; Huang, Y.; Sun, B.; Liao, Q.; Lu, H.; Jian, B.; Mohrbacher, H.; Zhang, W.; Guo, A.; Zhang, Y. Effect of Nb on hydrogen-induced delayed fracture in high strength hot stamping steels. *Mater. Sci. Eng. A* **2015**, *626*, 136–143. [CrossRef]
60. Ejaz, A.; Lu, Z.; Chen, J.; Xiao, Q.; Ru, X.; Han, G.; Shoji, T. The effects of hydrogen on anodic dissolution and passivation of iron in alkaline solutions. *Corros. Sci.* **2015**, *101*, 165–181. [CrossRef]
61. Rehrl, J.; Mraczek, K.; Pichler, A.; Werner, E. The Impact of Nb, Ti, Zr, B, V, and Mo on the Hydrogen Diffusion in Four Different AHSS/UHSS Microstructures. *Steel Res. Int.* **2014**, *85*, 336–346. [CrossRef]
62. Wallaert, E.; DePover, T.; Arafin, M.; Verbeken, K. Thermal Desorption Spectroscopy Evaluation of the Hydrogen-Trapping Capacity of NbC and NbN Precipitates. *Met. Mater. Trans. A* **2014**, *45*, 2412–2420. [CrossRef]
63. Wang, S.; Yang, S.; Gao, K.; He, X. Corrosion Resistance of low alloy weathering steel in chloride-containing environment. *J. Mater. Heat Treat.* **2008**, *29*, 170–175. [CrossRef]
64. Guo, J.; Yang, S.; Shang, C.; Wang, Y.; He, X. Influence of carbon content and microstructure on corrosion behaviour of low alloy steels in a Cl− containing environment. *Corros. Sci.* **2009**, *51*, 242–251. [CrossRef]
65. Wang, Z.; Huang, Y.; Li, J.; Yang, L.; Xie, D. Effect of Nb on the corrosion behavior of X80 steel welding heat affected zone in simulated seawater. *Chin. J. Corros. Prot.* **2016**, *36*, 7. [CrossRef]
66. Xue, W.; Li, Z.; Xiao, K.; Yu, W.; Song, J.; Chen, J.; Dong, C.; Li, X. Initial microzonal corrosion mechanism of inclusions associated with the precipitated (Ti, Nb)N phase of Sb-containing weathering steel. *Corros. Sci.* **2020**, *163*, 108232. [CrossRef]
67. Yue, Y.; Tang, D.; Wu, H.; Liang, J.; Ju, B. Effect of Nb on corrosion properties of low-alloy steel in strongly acidic solution environment with high Cl^-. *Mater. Eng.* **2015**, *43*, 14–20. [CrossRef]
68. Tyurin, A.G.; Pyshmintsev, I.Y.; Kostitsyna, I.V.; Zubkova, I.M. Thermodynamics of chemical and electrochemical stability of corrosion active nonmetal inclusions. *Prot. Met.* **2007**, *43*, 34–44. [CrossRef]
69. Szklarska-Smialowska, Z. Influence of Sulfide Inclusions on the Pitting Corrosion of Steels. *Corrosion* **1972**, *28*, 388–396. [CrossRef]
70. Wranglen, G. Pitting and sulphide inclusions in steel. *Corros. Sci.* **1974**, *14*, 331–349. [CrossRef]
71. Williams, D.E.; Kilburn, M.; Cliff, J.; Waterhouse, G. Composition changes around sulphide inclusions in stainless steels, and implications for the initiation of pitting corrosion. *Corros. Sci.* **2010**, *52*, 3702–3716. [CrossRef]
72. Avci, R.; Davis, B.; Wolfenden, M.; Beech, I.; Lucas, K.; Paul, D. Mechanism of MnS-mediated pit initiation and propagation in carbon steel in an anaerobic sulfidogenic media. *Corros. Sci.* **2013**, *76*, 267–274. [CrossRef]
73. Ke, R.; Alkire, R. ChemInform Abstract: Initiation of Corrosion Pits at Inclusions on 304 Stainless Steel. *ChemInform* **1996**, *27*, 4056–4062. [CrossRef]
74. Ke, R.; Alkire, R. Surface Analysis of Corrosion Pits Initiated at MnS Inclusions in 304 Stainless Steel. *J. Electrochem. Soc.* **1992**, *139*, 1573–1580. [CrossRef]

75. Park, I.-J.; Lee, S.-M.; Kang, M.; Lee, S.; Lee, Y.-K. Pitting corrosion behavior in advanced high strength steels. *J. Alloys Compd.* **2015**, *619*, 205–210. [CrossRef]
76. Zhou, Y.; Wang, Y.; Zheng, S.; Zhang, B.; Ma, X. Strain-induced preferential dissolution at the dislocation emergences in MnS: An atomic scale study. *Philos. Mag.* **2015**, *95*, 2365–2375. [CrossRef]
77. Wei, J.; Dong, J.; Ke, W.; He, X. Influence of Inclusions on Early Corrosion Development of Ultra-Low Carbon Bainitic Steel in NaCl Solution. *Corrosion* **2015**, *71*, 1467–1480. [CrossRef]
78. Al-Negheimish, A.; Alhozaimy, A.; Hussain, R.R.; Al-Zaid, R.; Singh, J.; Singh, D. Role of Manganese Sulfide Inclusions in Steel Rebar in the Formation and Breakdown of Passive Films in Concrete Pore Solutions. *Corrosion* **2014**, *70*, 74–86. [CrossRef]